Steady-shear-enhanced microdiffusion with multiple time scales of confined, mesoscopic, two-dimensional dusty-plasma liquids

Chong-Wai Io and Lin I
Department of Physics and Center for Complex Systems, National Central University, Chungli, Taiwan 32054, Republic of China
(Received 29 March 2009; published 4 September 2009)

We experimentally investigate the multitime scale diffusion and the spatiotemporal behaviors of the degrees of enhancement for the longitudinal and the transverse diffusions in a confined mesoscopic quasi-two-dimensional dusty-plasma liquid sheared by two parallel counterpropagating laser beams. The steady external drive directly enhances the longitudinal cooperative hopping, associated with the shear bands that have high shear rate near boundaries. It drastically excites the slow hopping modes to high fluctuation level in the outer band region, accompanied by the enhanced superdiffusion. Through cascaded many-body interaction, the excitation flows from the outer region toward the center region, from the longitudinal modes to the transverse mode, and from the slow hopping modes to the fast caging modes, which are in better contact with the thermal bath. It causes the weaker enhancement of fluctuation level, and diffusion for the center region and the fast modes. The boundary confinement further breaks the system symmetry and enhances anisotropy. It has much stronger effect on the suppression of the transverse hopping modes than the longitudinal hopping mode. The degrees of enhancement of the fluctuations by the shear stress are highly anisotropic for the large amplitude slow modes, especially in the outer region but are more isotropic in the inner band.

DOI: 10.1103/PhysRevE.80.036401 PACS number(s): 52.27.Lw, 66.20.−d, 05.40.−a

I. INTRODUCTION

Microscopically, the cold liquid can be treated as a coupled many-body network under moderate stochastic thermal kicks, and exhibits multitime scale dynamics [1–4]. Applying steady opposite shear stresses along the two opposite parallel boundaries of a confined liquid induces steady viscous deformation and drives the system out of thermal equilibrium. The momentum from persistent shear drive is dissipated through the network from the boundary to the center to enhance fluctuations and diffusivities at different time scales. If the liquid width goes down to the molecular scale, the boundary confinement plays an important role on breaking the system symmetry and introduces anisotropy for micromotion [4–13]. Nevertheless, the small molecular scale of the real liquid hinders the direct observation of shear enhanced transport at the discrete kinetic level. In this work, we experimentally investigate anisotropic multitime scale microdiffusion, enhanced by the steady shear in confined mesoscopic quasi-two-dimensional (2D) dusty-plasma liquids through directly tracking particle micromotion.

Microscopically, the shear-free 2D cold liquid melted from a triangular lattice type structure is still tightly packed. Each particle is surrounded by about six nearest neighbors. The particle motion is constrained by the caging potential well formed by the nearest neighbors. At short-time scale, the insufficient thermal agitation makes most particles exhibit small amplitude *caged oscillation* in the caging well. After accumulating sufficient constructive thermal perturbation over a longer time scale, some particles can surmount the caging barriers and exhibit persistent hopping to the new caging sites, and wait for their next hopping. Therefore, the multitime scale microdynamics is dominated by the small amplitude motion at the short-time scale, the superdiffusion for the intermediate time scale that is longer than the accumulating time scale for the onset of persistent hopping. The diffusion is nearly normal at the time scale that is longer than the typical time interval for a single persistent hopping, which washes out the motion memory [1–4]. The strong mutual coupling makes hopping occur cooperatively involving a small number of particles [1–4]. Applying external stress directly enhances the persistent hopping [4,14,15]. Recent theoretical studies in cold liquids and glassy systems predicted that the persistent external stress first excites the hopping dominated slow mode (α relaxation) to larger fluctuation level [16,17]. In addition to the spatial propagation, the energy flows to the small amplitude fast caging modes, which are in better thermal contact with the background thermal bath at lower temperature [16,17]. However, this has not been demonstrated experimentally at the discrete level.

Unlike the Newtonian liquid with constant viscosity, a sheared thin liquid confined in a mesoscopic gap about a few interparticle distance in width exhibits anisotropic micromotion and shear banding with high shear rate in the outer bands [4–6,8,10,12,13]. The above behaviors reflect the nonlinear and nonuniform dynamical response of the system under the interplay of boundary confinement, mutual interaction, thermal agitation, and external stress. The boundary has two competing effects. On one hand, its topological constraint directly suppresses transverse hopping, which makes the microtransport anisotropic and forms layered microstructures with better structural ordering near the boundary [4–13]. On the other hand, the boundary is a source region for pumping in longitudinal momentum from the external stress. It induces higher local shear rate in the outer band and enhances fluctuations that gradually spread to the inner band with small shear rate [12]. The induced shear banding with nonuniform shear-rate profile further complicates the spatial distribution of the transverse and the longitudinal diffusivities and their scaling behaviors at different time scales.

The dusty-plasma liquid composed of micrometer sized particles that are negatively charged and suspended in a low-

pressure glow discharge provides a good platform to address the above issues through direct visualization at the discrete level [18–20]. In the past decade, the microdynamics in dusty-plasma liquids such as: the multitime scale non-Gaussian diffusion and defect dynamics [2–4,21–25], the shear enhanced vortex formation, shear banding and thinning, and viscosity measurement for liquids under the steady shear [12,14,15,26–28], scanning laser induced heating and superdiffusion [27–31], confinement induced layering and slow dynamics [13], etc., to name a few, have been studied. For example, driven out of thermal equilibrium by two opposite fast scanning laser beams, heating associated with energy flow from the fast mode to the slow mode has been observed [28]. In another experiment, the heat transfer rates along and normal to the directions of the scanning laser beam on a monolayer dust plasma crystals were found to be different [31]. Nevertheless, the following issues that are important for both nanoscience and technology have never been addressed for the liquid in the mesoscopic gap: (a) the confinement effect on the nonuniform and anisotropic microdiffusions, and their scaling behaviors for the *shear-free* liquid at different time scales and different distances to the boundary. (b) The effect of the steady shear on the spatiotemporal microtransport through cascading the excitation from the boundary to the center, from slow modes to fast modes, and from the longitudinal to the transverse directions.

In this work, we investigate the above two unexplored issues using a thin quasi-2D dusty-plasma liquid, confined in a narrow gap and sheared by two counterpropagating laser beams along the opposite boundaries. The particle mean velocities and the mean-square displacements (MSDs) (in the mean drifting frame) along the two orthogonal directions at different time scales, different normal distance from the boundary, and different shear stresses (laser powers) are measured. We first address the scaling behaviors of multitime diffusion for the shear-free thin liquid, and find that the intermediate and the long-time diffusivities both along the transverse and longitudinal directions are suppressed by the boundary confinement but with different suppression degrees. The long-time transverse motion for the outmost layer is subdiffusive. We then find that, under shear stress, the enhancement degree of the longitudinal fluctuation is much higher in the outer shear band region with high shear rate, and nonlinearly decays toward the center region with low shear rate. The enhancement degree is large for the slow mode, gradually decays with decreasing time scale, and is negligible for the fast caging mode, associated with the extension of the stronger superdiffusion from the intermediate time to the long-time regime. The enhancement degree is more anisotropic for the slow modes, especially for the outer band, due to the direct momentum pumped in along the longitudinal direction and the transverse topological confinement of the boundary, which directly suppresses the transverse hopping.

II. EXPERIMENT

The experiment is conducted in a cylindrical symmetric rf dusty-plasma system. A weakly ionized discharge (n_e $\sim 10^9$ cm^{-3}) is generated in 330 mTorr Ar gas using a 14 MHz rf power system operated at 2.0 W. The suspended and negatively charged ($\sim 5000e$/particle) melamine-formaldehyde particles 6 μm in diameter are confined by the strong electric field in the surrounding dark space (sheath) adjacent to the two parallel vertical glass confining plates 38 mm in length and 14 mm in height on the center region of the bottom electrode. The length, width, and the thickness of the dust cloud are 26, 2.1 and 1.7 mm, respectively. This quasi-2D liquid has slipping boundaries. Vertically, the suspended dust particles (about eight particles in each chain) are aligned through the wake field effect of the downward ion flow [32]. Particles in the same chain move together horizontally. As shown in the sketch of Fig. 1, two parallel and counterpropagating cw laser sheets (488 nm Ar^+ laser) with 0.4 mm in half width and 2.5 mm in height (covering the entire vertical chain) are introduced horizontally to push the two outmost rows of particles near each boundary. The shear stress is linearly proportional to the laser power. The chain positions in the horizontal plane are illuminated by a thin laser sheet (0.2 mm in thickness and $\lambda = 532$ nm) and monitored through video microscopy. The mean interchain distance a is 0.3 mm. For the statistics of the run at each laser power, 5 min of video data at 30 Hz sampling rate are used. The spatial resolution of the charge-coupled device (CCD) camera (640×480 pixels for each frame) is about 38 pixel per a. The size of the field of view of each video frame is 5×3.8 mm^2, which contains about 170 dusts in the horizontal plane. The sequential video images are digitally processed to track the particle positions and obtain the particle displacements in different time intervals.

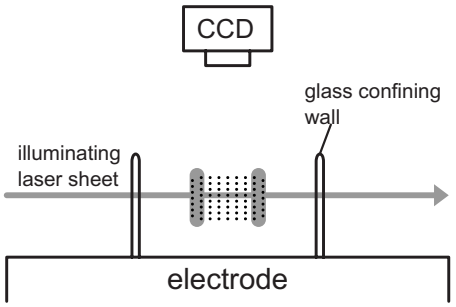

FIG. 1. The sketch of the end view of the experimental setup. The dust cloud is levitated by the sheath field and confined horizontally by sheath fields adjacent to the two vertical glass plates. Two counterpropagating (one into and the other one out of the viewing plane) laser beams as shown by the shaded regions are used to shear the suspended dust liquid. Dusts are vertically aligned by the downward flow. Dusts along the same vertical chain move together horizontally. The dust horizontal positions are illuminated by a thin horizontal laser ($\lambda = 532$ nm) sheet and monitored by a CCD camera mounted on the top.

III. RESULTS AND DISCUSSIONS

First, we plot particle trajectories (Fig. 2) to illustrate how particles move microscopically at different time scales and different laser powers (100 mW corresponds to 5.6

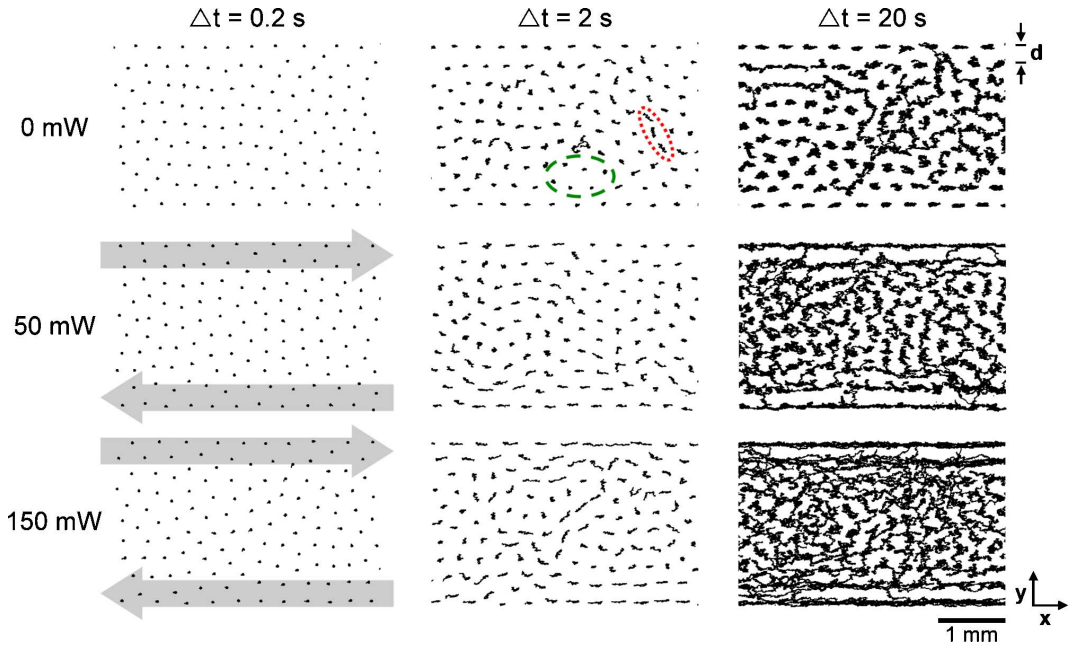

FIG. 2. (Color online) The particle trajectories at different time intervals and different laser powers. The gray arrows indicate the positions and the directions of the two parallel counter laser beams. At short-time scale (0.2 s), dusts exhibit small amplitude motion. After accumulating constructive thermal perturbation over longer time scale (2 s), some particles (e.g., the particles inside the dotted ellipse) exhibit persistent hopping surrounding the particles (e.g., the particles inside the dashed ellipse) exhibiting small amplitude caged oscillation. The motion becomes more disordered at $\Delta t=20$ s. In the two outmost layers, the confinement suppresses primarily on the long-time transverse motion and secondarily on the longitudinal hopping. Applying shear causes very little change on the small amplitude caged oscillation in the short-time scale, in which the motions are almost isotropic through the entire liquid. However, shear enhances the hopping dominated motions in the intermediate and the long-time regimes. The motion becomes highly anisotropic for the outer region.

$\times 10^{-11}$ dyn radiation force on each particle). At short-time scale (the left column of Fig. 2), the small amplitude motions are quite uniform and isotropic, regardless of changing the stress and the presence of boundaries. At the intermediate time scale (the center column of Fig. 2), the cooperate particle hopping (e.g., the trajectories inside the dotted ellipse in Fig. 2) and caged motion (the trajectories inside the dashed ellipse in Fig. 2) can be both observed. At the long-time scale (the right column of Fig. 2), particle motion becomes more disordered. The boundary confinement suppresses the transverse hopping motion in the outer band. The external stress enhances hopping, especially in the outer band.

We further divide the liquid into nine longitudinal layers. Each layer has width $d=\sqrt{\frac{3}{2}}\ a$ (Fig. 2), and transverse distance y from the center. Namely, $y=nd$ for layer n, and $n=0$ and ± 4 for the center and the outmost layers, respectively. The mean longitudinal velocity profiles at different laser powers are plotted in Fig. 3. The shear banding with higher shear rate in the two outmost layers than that in the center region becomes more obvious at the larger laser power.

A. Shear-free liquid

We use the shear-free liquid, starting from the longitudinal motion to the transverse motion, to construct a micropicture of the spatiotemporal behaviors of thermal excited particle micromotion under the interplay of mutual interaction and confinement. In addition to the particle trajectories shown in Fig. 2, particle mean-square displacement and the effective diffusivity at different time scales and different transverse distances from the center are used as important statistical measures for thermal induced motion. The microorigins of the observed behaviors are explained. The mean-square displacements along the **x** (longitudinal) and the **y** (transverse) directions of layer n, and in the time interval τ are defined as $\mathrm{MSD}_{x,y}(\tau,n)=\langle[\Delta r_{x,y}(\tau,n)]^2\rangle$ by measuring the particle displacement $\Delta r_{x,y}(\tau,n)$ along the **x** and the **y** directions in the mean drifting frame of layer n in the time interval τ. The corresponding effective diffusivity $D^e_{x,y}(\tau,n)$ is defined as $\mathrm{MSD}_{x,y}(\tau,n)/\tau$.

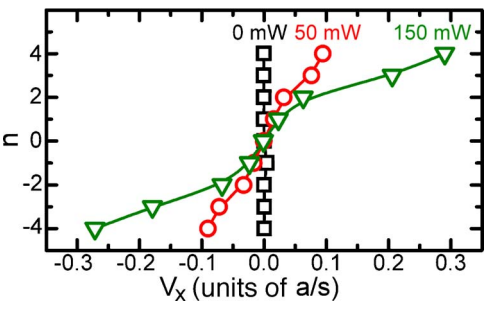

FIG. 3. (Color online) The averaged longitudinal velocity profile at different laser powers. The shear banding with high shear rate in the outer bands become more obvious at the larger laser power.

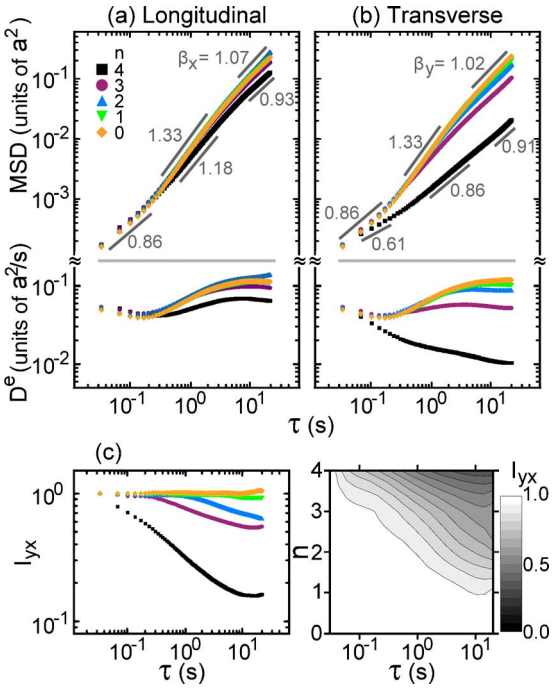

FIG. 4. (Color online) The plots of MSD and D^e versus τ of the different layers, at different transverse distance nd from the center, for (a) the longitudinal and (b) the transverse directions of the shear-free run. The gray lines and the corresponding numbers show the upper and lower bounds of the scaling exponents. (c) The plot of I_{yx} versus τ and n showing the spatial and temporal dependences of the isotropy of MSD (or D^e). The boundary confinement slightly suppresses the long-time longitudinal diffusion but strongly suppresses the transverse diffusion for the outmost layer.

1. Longitudinal diffusion

Figure 4(a) depicts the behavior of longitudinal mean-square displacement $\mathrm{MSD}_x(\tau,n)$. The cold liquid has mainly triangular lattice type ordered domains separated by defect clusters (not shown) [2,4,23]. Similar to the bulk liquid studied previously, at short-time scale ($\tau \leq 0.2$ s), the particle exhibits small amplitude caged fluctuation (Fig. 2) [2,4]. The caging leads to the subdiffusion with scaling exponent β_x of MSD_x slightly smaller than one for the short-time regime (note that due to the finite spatial resolution of the imaging system, the actual exponent could be slightly larger for the first three data points). In the intermediated time regime ($0.2\ \mathrm{s} < \tau < 4$ s), the motion is dominated by hopping after the accumulation of sufficient constructive perturbations from the background fluctuation. The persistent diffusion (superdiffusion) has $1.33 > \beta_x > 1.18$ from the center to the boundary layers for the intermediate τ. For the time scale that is longer than the typical hopping time scale ($\tau > 4$ s), the memory of hopping is lost. It leads to the normal diffusion with $\beta_x \simeq 1$. The effective diffusion coefficient $D_x^e(n,\tau)$ is also plotted in Fig. 4(a). It first slightly decreases, then increases in the intermediate time regime, and finally levels off in the long-time regime.

2. Spatial dependence and the anisotropy of diffusion

The boundary confinement adds extra topological constraint to the particle motion. It breaks the system symmetry and makes the diffusion anisotropic. It also affects the motion at different time scales. The curves of $\mathrm{MSD}_x(\tau)$ [and $D_x^e(\tau)$] for different n all nearly merge at the small τ limit and gradually fan out with increasing τ. The curves of $\mathrm{MSD}_x(\tau,n)$ [and $D_x^e(\tau,n)$] in the center region ($|n| \leq 2$) nearly collapse but are lower in the two outmost layers, especially at large τ. Note that the long-time diffusion for the outmost layer is subdiffusive with β_x about 0.93. Figures 4(b) and 4(c) show the plots of $\mathrm{MSD}_y(\tau)$, $D_y^e(\tau)$, and $I_{yx}(\tau)$ for different layers. $I_{yx}(\tau,n)$ is defined as $I_{yx}(\tau,n) = \mathrm{MSD}_y(\tau,n)/\mathrm{MSD}_x(\tau,n) = D_y^e(\tau,n)/D_x^e(\tau,n)$, and measures the isotropy of the degree of diffusivity. The diffusion is nearly isotropic over the entire τ for the center band ($n = 0, \pm 1$), but I_{yx} drastically drops from one as the displacement amplitude increases with increasing τ in the outer band. The dropping is most serious for the outmost layer.

The above observations evidence the primary (secondary) suppression effect of boundary confinement on the transverse (longitudinal) motion in the outer band, especially for the large amplitude motion. It makes the transverse diffusion antipersistent over the entire τ for the outmost layer regardless of the scale of the displacement amplitude. The confinement effect only extends to the transverse scale about the pair-correlation length, which is about $3a$ [11,12]. The transverse displacements of the second and the third outmost layers are also suppressed but with decreasing degree of suppression. In the outer band, the suppression of the transverse hopping significantly reduces the vortex type hopping rate and consequently induces the secondary suppression on the longitudinal hopping only in the outmost *two* layers. The 20 s trajectories of the shear-free run in Fig. 2 shows that the motion is highly anisotropic for the outmost layer, and the longitudinal motion also seldom occurs. However, for the small amplitude fast caged oscillations, both the longitudinal and the transverse motions are much less suppressed [also see Figs. 2 and 4(c)] even in the outer band. In the center band, even the long-time large amplitude hopping is also isotropic because of the large number of accessible pathways for the isotropic vortex type hopping.

B. Sheared liquid

After understanding the behaviors of the shear-free liquid, we switch to the behaviors of the sheared liquid. Similarly, we start from the behaviors of the longitudinal motion and then go to the behaviors of the transverse motion. In addition to measurements for the shear-free case, we further measure the degree of shear enhancements on the effective diffusivities along both directions to illustrate the effect of shear stress on the microexcitation.

1. Longitudinal motion

Figures 5(a) and 5(b) show the $\mathrm{MSD}_x(\tau,n)$ curves for the two sheared runs at 50 and 150 mW laser power, respectively. The degree of shear enhancement on the longitudinal diffusivity, $R_x(\tau,n)$, which is defined as the ratio of the $\mathrm{MSD}_x(\tau,n)$ [or $D_x^e(\tau,n)$] to that of the shear-free case, is also plotted [Figs. 5(c) and 5(d)]. At 50 mW laser power, the system shows weak shear banding with slightly nonuniform

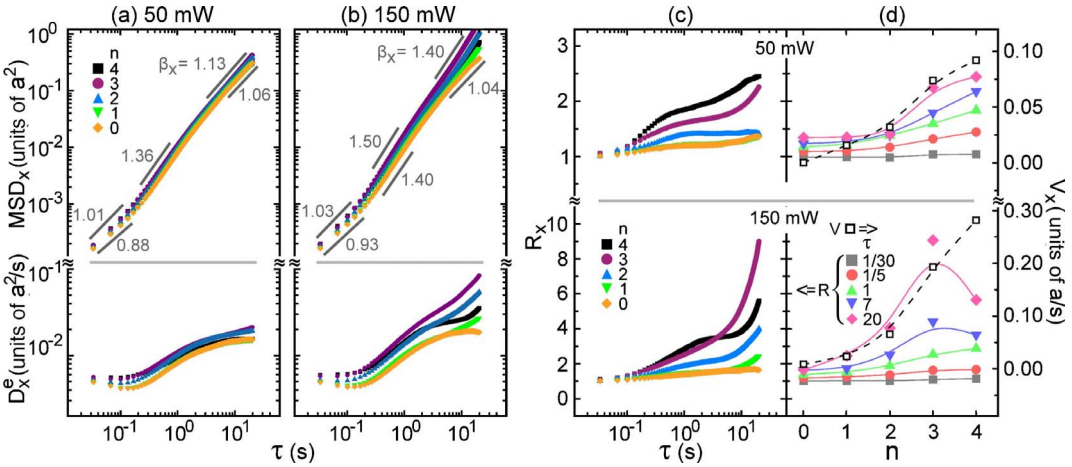

FIG. 5. (Color online) (a) and (b) The MSD_x and D_x^e (measured in the local mean drifting frame) versus τ plots for different n of the sheared runs at 50 and 150 mW laser power, respectively. The gray lines and the corresponding numbers show the upper and lower bounds of the scaling exponents. (c) and (d) The plots of R_x versus τ and n showing the degree of shear enhancement on fluctuations and the direction of the energy flow. The dash lines in (d) show the dependence of the mean longitudinal velocity v_x on n. Increasing the laser power makes the diffusion for the intermediate and long-time regimes more persistent (with large β), especially for the outer layers. The steady shear first excites the slow hopping mode and then the energy is transferred to the excitation of the fast caging mode. Spatially, under the competition of the boundary confinement and the energy pumped in from the outer band by the laser beam along the two outmost layers, the second outmost layer has the largest enhancement degree at large τ.

shear rate (Fig. 3). The shear banding becomes more pronounced, with a high shear-rate outer band, at 150 mW laser power. The following rules are found under the changes in τ, n, and laser powers: (i) at the smallest τ end (1/30 s), R_x [Figs. 5(c) and 5(d)] still remains at one regardless of the increasing n and laser power. (ii) With increasing τ, the spatial distribution of R_x in Fig. 5(d) changes from the nearly linear to the highly nonlinear profile. The deviation from the linear profile also increases with the increasing laser power. For $\tau > 1$ s, the nonlinear high R_x outer band coincides with the high shear-rate band. (iii) The scaling exponents β_x in the short-time, intermediate time, and long-time regimes all increase with the increasing power. The MSD_x curves are more straightened as n increases [Fig. 5(b)].

Now let us explain the observed stress effect on the longitudinal fluctuation enhancement. Applying external stress effectively tilts the caging well and enhances forward hopping. It directly feeds longitudinal momentum to the slow modes, which is then dissipated by exciting the fast caged oscillation or hopping of nearby particles in the surrounding network through cascaded mutual interaction. That is how the fluctuations are transferred from the slow to the fast modes and from the boundary to the center. Unlike the thermal induced hopping, which usually terminates when the particle travels one a after dissipating energy to the surrounding particles, the shear enhanced hopping can move faster, and persist over larger distance and longer time. It induces the earlier onset of persistent hopping and extends the superdiffusion from the intermediate time scale to the long-time scale [see the continuous rise of $D_x^e(\tau)$ even in the long-time regime in Fig. 5(b)]. The enhancement effect is most significant in the outer high shear-rate band, especially under the larger laser power [Fig. 5(c)]. It compensates the confinement suppression effect in the outer band, and makes the diverging $\mathrm{MSD}_x(\tau)$ curves with increasing τ of the shear-free case less diverging at 50 mW laser power and diverge again at 150 mW, after the crossing over of the second outmost curve. Unlike in the shear-free case where the long-time diffusion becomes nearly normal, the superdiffusion with β_x remaining greater than one in the long-time regime at the large laser power manifests that the system is driven far from thermal equilibrium by the large external shear.

How does the excitation flow from modes to modes at different time scales? The larger R_x at larger τ than that at the smaller τ indicates the energy flow from the slow modes with larger fluctuation levels to the fast modes. The fast modes are in better thermal contact with the thermal bath through the high rate dust-neutral collisions. Their small amplitude motion also suffers from negligible confinement suppression. Therefore, R_x at the small τ end stays close to one and has a nearly uniform transverse distribution regardless of the increasing laser power [Fig. 5(c)]. Similar energy flow from the slow (α relaxation) to the fast modes (β relaxation) was also obtained in the theoretical studies for the glassy system and cold liquid system driven by slow external shear [16,17]. In contrast, in another recent dusty-plasma liquid heating experiment, the energy transferred from the two opposite high rate scanning laser beams directly excite the high-frequency mode at frequency resonant with that of the scanning lasers [28]. The energy then cascades to other modes.

In addition to the energy flow from the slow modes to the fast modes shown in Fig. 5(c), how does the energy flow spatially? The spatial gradient of R_x along the transverse direction shown in Fig. 5(d) also supports the energy flow from the outer band with higher fluctuation enhancement to the center band with lower enhancement. Note that in the outer band with the higher shear rate, R_x and its gradient are both large, especially for the intermediate and large τ. The larger level of shear enhanced fluctuations at the second outmost

layer for the higher laser power case is also consistent with our previous finding of the higher structural rearrangement rate in the outer shear band [12]. Note that if we rescale the velocity profiles in Fig. 3 of the two sheared runs by the velocities of their outmost layers, the two rescaled profiles do not collapse (not shown). The 150 mW case shows stronger shear banding effect. It reveals that the shear banding in our confined liquid cannot be simply attributed to the local neutral friction as proposed in the linear fluid model using constant shear viscosity and neutral friction for the liquid sheared by two high intensity counter parallel laser beams in the center of region of a monolayer dusty plasma [15]. The higher shear rate in the outer band induces higher local energy dissipation rate. The subsequent larger fluctuating level weakens the caging effect, which promotes hopping and sustains the high shear rate in the outer band. This positive feedback process thereby sustains shear banding. This effect becomes more pronounced with the increasing stress.

2. Transverse motion

Finally, let us show the stress effect on the transverse fluctuation under transverse confinement, and mediated through direct particle motion and the interaction with the surrounding network. Intuitively, the longitudinal drive directly excites the longitudinal hopping. However, the particles near the boundary are not perfectly layered and cannot merely exhibit longitudinal sliding as in the case of graphite under shear. The shear induced forward hopping can be frustrated and turned into transverse hopping in the form of hopping vortices or strings through many-body interaction with the surrounding particle network. Namely, as manifested by the trajectories in Fig. 2, shear enhanced hopping is 2D in nature. Figures 6(a) and 6(b) show that increasing the external stress enhances MSD_y and D_y^e for all the layers. For the sheared run at 50 mW, the profiles of I_{yx} [Fig. 6(c)] in the center band are similar to those of the corresponding layers of the shear-free run for $\tau < 1$ s. It implies that the enhancement degree of fluctuations by shear is quite isotropic within the above time scale. Unlike extending the shear enhanced longitudinal superdiffusion to the long-time regime, the transverse diffusion of the outmost layer has $\beta_y \simeq 1$, in the long-time regime, because the confinement suppresses the large amplitude persistent transverse hopping. Therefore, the tails of the I_{yx} curves ($n \geq 3$) of the sheared runs bend down with increasing τ. This effect is more seriously enhanced as laser power increases to 150 mW. It can be further manifested by the highly anisotropic long-time (20 s) trajectories in the outer bands shown in Fig. 2. Note that I_{yx} curves in the center region ($n=0, \pm 1$) remain similar to those in the shear-free and the 50 mW runs for $\tau < 1$ s but the downward bending becomes more serious in the long-time regime in which the displacement has larger amplitude.

The above findings further support that the degrees of enhancement for the transverse excitations of the large amplitude slow modes in the outer layers by the slow drive is weaker than those of the longitudinal slow modes because the boundary confinement has the primary suppression effect on the transverse displacement but the momentum from the external stress has the primary enhancement effect on the longitudinal displacement, and is then converted to the transverse direction. These effects gradually decrease with decreasing n but is not negligible for the inner band, when the transverse displacement amplitude is large (i.e., at larger τ). For the outmost layer, the strongest confinement suppression of the transverse displacement also limits the longitudinal enhancement degree [see the dropping of R_x for the outmost layer in Fig. 5(c)]. However, through the cascaded many-body interaction, the enhancement degree becomes more isotropic for all the modes in the center layer, where there are more accessible pathways for the isotropic string or vortex type hopping.

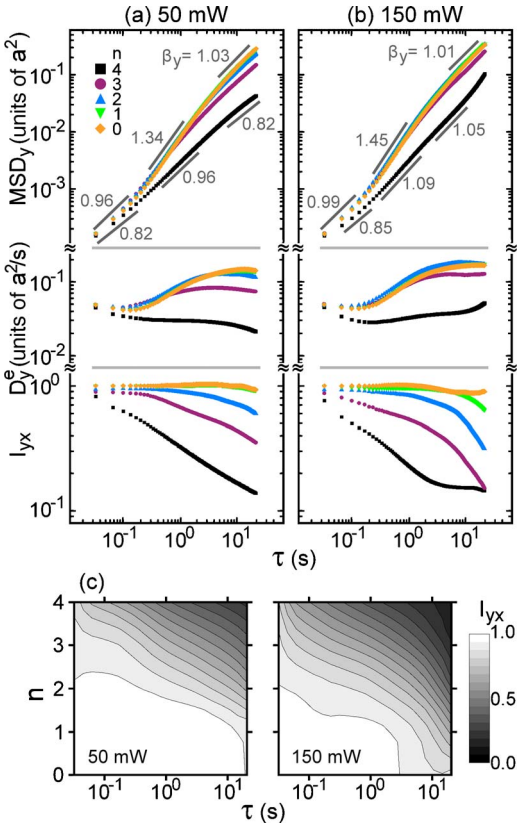

FIG. 6. (Color online) (a) and (b) The MSD_y and D_y^e (measured in the mean drifting frame) versus τ plots for different n of the sheared runs at 50 and 150 mW, respectively. The gray lines and the corresponding numbers show the upper and lower bounds of the scaling exponents. (c) The plot of I_{yx} versus τ and n showing the spatial and temporal dependences of the isotropy of MSD (or D^e). Similar to the longitudinal diffusion, increasing shear also increases the transverse diffusion. However, the confinement suppresses the enhancement degree for the outmost two layers. This effect also gradually decreases as n and τ decreases. Namely, the transfer of the longitudinal momentum from the steady shear to the fluctuation becomes more isotropic as energy is cascaded from the slow to the fast mode and from the outer to the center regions through many-body interactions and 2D hopping.

IV. CONCLUSION

In conclusion, we investigate the effects of boundary confinement and steady shear on the multitime scale microdiffu-

sion of the mesoscopically confined quasi-2D dusty-plasma liquid. The interplay of many-body interaction and thermal agitation makes the system exhibit multitime scale diffusion. The steady shear breaks the symmetry through pumping in persistent longitudinal momentum. Through cascaded interaction, it enhances fluctuations from the boundaries to the center, from the longitudinal direction to the transverse direction, and from the slow modes to the fast modes. The confinement has primary (secondary) suppression effect on the large amplitude transverse (longitudinal) motion. The major findings are listed as follows. (a) For the shear-free liquid, the alternate caged and hopping motions lead to the transition from the superdiffusion to the nearly normal diffusion with increasing time in the center region. In the outer region, the confinement suppression is more serious for the transverse motion, and makes the long-time diffusion subdiffusive for both directions. In the center band, the diffusion at all time scales remains nearly unaffected and isotropic. The small amplitude caged high-frequency oscillation is isotropic and uniform over the entire liquid. (b) Applying steady external shear extends the superdiffusion to the long-time regime, and makes the scaling exponents deviated further away from one over the entire liquid. The spatial and temporal distribution of $R_x(\tau,n)$ evidences that the fluctuating energy from the external stress flows from the boundary to the center and from the slow modes to the fast modes through cascaded many-body interaction, which frustrates the shear induced forward hopping, and induces further disordered fluctuations at different time scales in the surrounding network. The very small increase in R_x from one for the fast modes at the short-time extreme even at the high stress reveals the better thermal contact of the fast modes with the background thermal bath through neutral collisions. (c) The spatial and temporal distribution plots of I_{yx} show that the enhancement degrees for the slow longitudinal modes strongly increase in the outer shear band with the increasing shear rate. The strong suppression of the transverse hopping by the boundary confinement makes the enhancement degree of transverse motion by shear much weaker than that along the longitudinal direction for the slow mode, especially moving toward the boundary. In the center of the small τ regime, the many-body randomization process washes out the anisotropic effects of the boundary confinement and shear stress, and makes I_{yx} close to one.

ACKNOWLEDGMENT

This work is supported by the National Science Council of the Republic of China under Contract No. NSC96-2112-M-008-012-MY3.

[1] E. R. Weeks, J. C. Crocker, A. C. Levitt, A. Schofield, and D. A. Weitz, Science **287**, 627 (2000).
[2] Y. J. Lai and L. I, Phys. Rev. Lett. **89**, 155002 (2002).
[3] W. T. Juan and L. I, Phys. Rev. Lett. **80**, 3073 (1998).
[4] C. L. Chan, C. W. Io, and L. I, Contrib. Plasma Phys. **49**, 215 (2009).
[5] S. Granick, Phys. Today **52**(7), 26 (1999).
[6] B. Bhushan, J. N. Israelachvili, and U. Landman, Nature (London) **374**, 607 (1995).
[7] C. L. Rhykerd, Jr., M. Schoen, D. J. Diestler, and J. H. Cushman, Nature (London) **330**, 461 (1987).
[8] P. A. Thompson, G. S. Grest, and M. O. Robbins, Phys. Rev. Lett. **68**, 3448 (1992).
[9] J. Gao, W. D. Luedtke, and U. Landman, Phys. Rev. Lett. **79**, 705 (1997).
[10] M. Heuberger, M. Zach, and N. D. Spencer, Science **292**, 905 (2001).
[11] L. W. Teng, P. S. Tu, and L. I, Phys. Rev. Lett. **90**, 245004 (2003).
[12] C. L. Chan, W. Y. Woon, and L. I, Phys. Rev. Lett. **93**, 220602 (2004).
[13] G. Piacente, I. V. Schweigert, J. J. Betouras, and F. M. Peeters, Phys. Rev. B **69**, 045324 (2004).
[14] W. T. Juan, M. H. Chen, and L. I, Phys. Rev. E **64**, 016402 (2001).
[15] V. Nosenko and J. Goree, Phys. Rev. Lett. **93**, 155004 (2004).
[16] L. F. Cugliandolo, J. Kurchan, and L. Peliti, Phys. Rev. E **55**, 3898 (1997).
[17] L. Berthier, J. L. Barrat, and J. Kurchan, Phys. Rev. E **61**, 5464 (2000).
[18] J. H. Chu and L. I, Phys. Rev. Lett. **72**, 4009 (1994).
[19] H. Thomas, G. E. Morfill, V. Demmel, J. Goree, B. Feuerbacher, and D. Mohlmann, Phys. Rev. Lett. **73**, 652 (1994).
[20] P. K. Shukla and A. A. Mamun, *Introduction to Dusty Plasma Physics* (Institute of Physics Publishing, Bristol, 2002).
[21] B. Liu and J. Goree, Phys. Rev. E **75**, 016405 (2007).
[22] C. Reichhardt and C. J. Olson Reichhardt, Phys. Rev. Lett. **90**, 095504 (2003).
[23] W. Y. Woon and L. I, Phys. Rev. Lett. **92**, 065003 (2004); Y. H. Huang and L. I, Phys. Rev. E, **76**, 016403 (2007).
[24] B. Liu, J. Goree, and O. S. Vaulina, Phys. Rev. Lett. **96**, 015005 (2006).
[25] S. Nunomura, D. Samsonov, S. Zhdanov, and G. Morfill, Phys. Rev. Lett. **96**, 015003 (2006).
[26] Z. Donko, J. Goree, P. Hartmann, and K. Kutasi, Phys. Rev. Lett. **96**, 145003 (2006).
[27] S. Ratynskaia, K. Rypdal, C. Knapek, S. Khrapak, A. V. Milovanov, A. Ivlev, J. J. Rasmussen, and G. E. Morfill, Phys. Rev. Lett. **96**, 105010 (2006).
[28] V. Nosenko, J. Goree, and A. Piel, Phys. Plasmas **13**, 032106 (2006).
[29] V. Nosenko, S. Zhdanov, A. V. Ivlev, G. Morfill, J. Goree, and A. Piel, Phys. Rev. Lett. **100**, 025003 (2008).
[30] B. Liu and J. Goree, Phys. Rev. Lett. **100**, 055003 (2008).
[31] S. Nunomura, D. Samsonov, S. Zhdanov, and G. Morfill, Phys. Rev. Lett. **95**, 025003 (2005).
[32] See, e.g., M. Nambu, S. V. Valdimirov, and P. K. Shukla, Phys. Lett. A **203**, 40 (1995).